Title: Electrophysical properties of the multiferroic PFN-ferrite composites obtained by spark plasma sintering and classical technology

Author: Przemysław Niemiec, Joanna A. Bartkowska,·Dagmara Brzezińska,·Grzegorz Dercz,·Zbigniew Stokłosa

Citation style: Niemiec Przemysław, Bartkowska Joanna A.,·Brzezińska Dagmara,·Dercz Grzegorz, Stokłosa Zbigniew. (2020). Electrophysical properties of the multiferroic PFN-ferrite composites obtained by spark plasma sintering and classical technology. “Applied Physics A” (Vol. 126, iss. 11, 2020, art. no. 831, s. 1-8), DOI:10.1007/s00339-020-04024-0

Applied Physics A (2020) 126:831
https://doi.org/10.1007/s00339-020-04024-0

Applied Physics A
Materials Science & Processing

Electrophysical properties of the multiferroic PFN–ferrite composites obtained by spark plasma sintering and classical technology

Przemysław Niemiec[1] · Joanna A. Bartkowska[1] · Dagmara Brzezińska[1] · Grzegorz Dercz[1] · Zbigniew Stokłosa[1]

Received: 27 June 2020 / Accepted: 25 September 2020

Abstract
The multiferroic (ferroelectric–ferromagnetic) composites (PFN–ferrite) based on ferroelectromagnetic $PbFe_{1/2}Nb_{1/2}O_3$ powder and ferrite powder (zinc–nickel ferrite, $NiZnFeO_4$) were obtained in the presented study. The ceramic PFN–ferrite composites consisted of 90% powder PFN material and 10% powder $NiZnFeO_4$ ferrite. The ceramic powders were synthesized by the classical technological method using powder calcination, while densification of the composite powders (sintering) was carried by two different methods: (1) free sintering method (FS) and (2) spark plasma sintering (SPS). The composite PFN–ferrite samples were thermally tested, including DC electrical conductivity and dielectric properties. Besides, XRD, SEM, EDS (energy-dispersive spectrometry) and ferroelectric properties (hysteresis loop) of the composite samples were tested at room temperature. At the work, a comparison was made for the results measured for PFN–ferrite composite samples obtained by two methods. The X-ray examination of multiferroic ceramic composites confirmed the occurrence of the strong diffraction peaks derived from ferroelectric (PFN) matrix of composite as well as weak peaks induced by the ferrite component. At the same time, the studies showed the absence of other undesired phases. The results presented in this work revealed that the ceramic composite obtained by two different technological sintering methods (free sintering method and spark plasma sintering technique) can be the promising materials for functional applications, for example, in sensors for magnetic and electric fields.

Keywords Multiferroics · Ferroelectric–ferromagnetic composites · PFN ceramics · Ferrites

1 Introduction

Multiferroic materials (including multiferroic ceramic composites) exhibit at least two types of ferroic properties. In the case of ferroelectromagnetics, the magnetic phase exhibits magnetostrictive properties, whereas the electric one shows ferroelectric and/or piezoelectric properties [1–7]. Combining these types of materials into one (also to form a composite) allows changing the magnetic properties by applying an external electric field, or vice versa, changing the electrical properties with a magnetic field. An important issue in this type of applications is to obtain the greatest coupling coefficient of these two phases the so-called magnetoelectric coupling, on which the functional application of the materials depends [8–11]. According to the classification, made by D. Khomsky, the mutliferroic materials can be divided into multiferroics of type-I (with weak magnetoelectric coupling) and type-II (strong coupling of the magnetic and electric subsystems) [12]. Piezoelectric materials [13, 14] and ceramic composites with multiferroic properties are very promising materials for functional applications in modern microelectronics, for example, as sensors, actuators, piezotransducers, microwave and read/write devices, multiferroic memories, and multi-layer ceramic capacitors (MLCC) [15–19].

Many works appeared in the recent time on the preparation and properties of multiferroic composites [20–24] and multiferroic solid solutions [25, 26]. Also, in many works, the authors present the results of research on ceramic materials obtained in spark plasma sintering (SPS) technology, whose electrophysical properties are much better than for ceramic samples obtained in other technologies [27–30]. However, not all materials achieve satisfactory results of their final properties. This work is aimed to obtain

✉ Przemysław Niemiec
przemyslaw.niemiec@us.edu.pl

[1] Faculty of Science and Technology, Institute of Materials Engineering, University of Silesia in Katowice, 75 Pułku Piechoty 1a, 41-500 Chorzow, Poland

ferroelectromagnetic ceramic composites using the SPS sintering method and compare the test results with those obtained for ceramic materials prepared by classical method.

The study presents the properties of multiferroic composites based on PFN material and ferrite $NiZnFeO_4$. The composites were obtained via Spark Plasma Sintering method and classical technology. $PbFe_{1/2}Nb_{1/2}O_3$ (PFN) material which represents ferroelectromagnetic properties, has a perovskite-type structure with a general formula of ABO_3, where Pb ions locates in the A positions, while Fe and Nb ions randomly occupy B positions [31–38]. The magnetic properties were provided by nickel–zinc soft ferrite with the chemical composition of NiZnFeO4. The percentage of individual components in the composite was as follows: PFN—90%; ferrite—10%.

2 Experimental

2.1 Technology process

The main component of the multiferroic composite material was $PbFe_{1/2}Nb_{1/2}O_3$ (PFN). The PFN ceramic powder was prepared by the two-stage columbite method [39] wherein the starting oxides were PbO (99.99%, POCH), Nb_2O_5 (99.9%, Sigma-Aldrich) and Fe_2O_3 (99.9%, POCH). In the first step, the $FeNbO_4$ component was synthesized from a mixture of the oxides: Fe_2O_3 and Nb_2O_5 at following conditions: $T = 1000$ °C, $t = 4$ h, while, in the second step, a mixture of the $FeNbO_4$ and PbO powders were calcined at following conditions: $T = 800$ °C, $t = 3$ h. In the technological process, the ceramic powders were milled in a planetary mill FRITSCH Pulverisette 6 for 24 h in ethanol using zirconium balls.

In the case of the ferrite material ($Ni_{0.64}Zn_{0.36}Fe_2O_4$), starting oxides NiO (99.99%, Aldrich), ZnO (99.99%, POCH) and Fe_2O_3 (99.98%, Sigma-Aldrich) were milled under the same conditions. The ferrite powder was obtained by calcination at 1000 °C for 4 h.

To obtain the ferroelectric–ferromagnetic material, the ceramic PFN powder was mixed with ferrite powder in the weight ratio of 9:1 (planetary mill, wet method in ethanol, for 8 h) and calcined at 900 °C for 2 h. The ceramic composites were obtained by the (1) free sintering method (FS) and (2) spark plasma sintering (SPS) methods. In the first one, the ceramic sample densification was carried out at 1050 °C for 2 h (CMc sample). In the case of the spark plasma sintering method, the ceramic sample was treated at $T_{SPS} = 800$ °C for $t_{SPS} = 3$ min under applied pressure $p_{SPS} = 50$ MPa (SPSc sample).

The final steps of the technological process of the PFN–F ceramic composites were grinding, polishing, removing mechanical stresses (annealing) and next putting silver paste electrodes on the both composite sample surfaces.

2.2 Investigations

In the first method, the temperature synthesis of the PFN–F ceramic powder was appointed on the basis of differential thermal analysis DTA (TG) tests using a Q-1500D derivatograph (not presented here).

The XRD test of the composite powder was carried out at room temperature on a diffractometer by Phillips (PANalytical, Phillips X'Pert Pro). The X-ray diffraction patterns were recorded over the range of $2\theta = 10$–$65°$ in step-scan mode: 0.05 degrees and 4 s/step and the copper radiation CuKα was used. The SEM patterns of the composite samples were carried out by a scanning electron microscope JSM-7100F TTL LV (Jeol Ltd., Tokyo, Japan). For SEM and EDS tests, the samples were coated with gold to provide electrical conductivity and avoid charging effects. The temperature dielectric measurements were made on a capacity bridge LCR Meter (Quad Tech 1929 Precision LCR Meter, Quad Tech, Inc. Maynard, USA), in the temperature range of 20–180 °C (heating rate of 1.0°/min, frequency range of 0.02–100 kHz). The temperature measurements of DC electric conductivity were made using a Keithley 6517B electrometer (Keithley Instruments, Cleveland, OH, USA), in the temperature range of 20–400 °C (a heating cycle). The hysteresis (*P*–*E*) loops were recorded at room temperature using a Sawyer–Tower circuit and a high-voltage amplifier (Matsusada Inc. HEOPS-5B6 precision, Matsusada Precision Inc., Kusatsu, Japan) at 1 Hz [40]. The data were stored on a computer disc using an A/D, D/A transducer card (National Instruments Corporation, Austin, TX, USA) and the LabView computer program.

The magnetic properties were obtained using a SQUID magnetometer (MPMS XL-7 Quantum Design) in the temperature range of − 271 to 27 °C (magnetic field to 7 T) and a magnetic Faraday scale in the temperature range of 27–600 °C.

3 Results and discussion

The X-ray diffraction patterns of PFN–F material are displayed in Fig. 1. In the case of CMc sample (Fig. 1a), the analysis showed the occurrence of the strong peaks derived from PFN ferroelectric matrix of composite sample as well as week peaks coming from the ferrite component ($Ni_{0.64}Zn_{0.36}Fe_2O_4$). The best fit to the diffraction peaks of PFN component was obtained for JCPDS card no. 01-076-6488 pattern (tetragonal perovskite structure, P4mm space group) [41]. In the case of the ferrite component, the diffraction pattern shows a typical cubic spinel phase—JCPDS

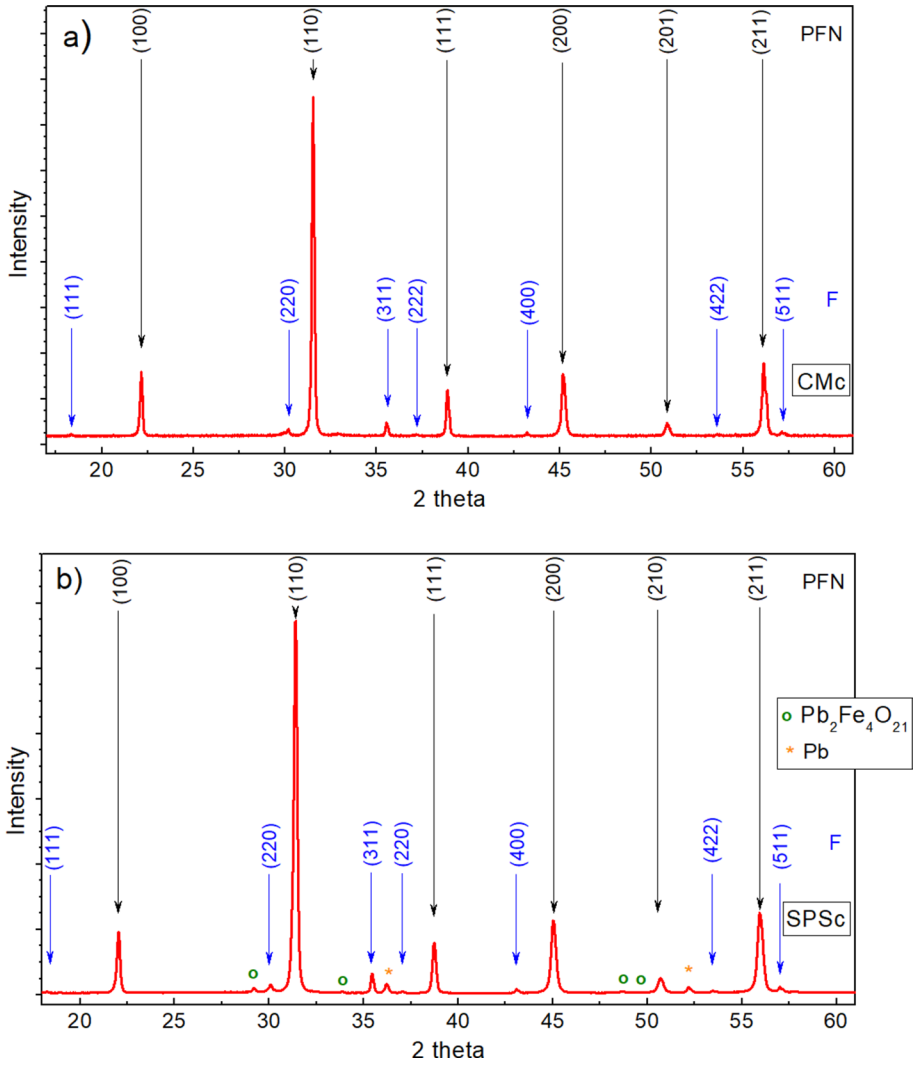

Fig. 1 X-ray diffraction patterns of the multicomponent PFN–F composite materials: **a** CMs, **b** SPSc

card no. 01-077-9717 (Fd-3 m) [42]. The XRD test at room temperature has not shown the presence of foreign phases.

In the case of SPSc sample (Fig. 1b), the XRD patterns showed strong peaks attributed to two main phases of the PFN–F composite, i.e., PFN (JCPDS card no. 01-076-6488) and ferrite $Ni_{0.64}Zn_{0.36}Fe_2O_4$ (JCPDS card no. 01-077-9717). However, the analysis also showed the presence of foreign phases (to a small extent), i.e., the $Pb_2Fe_4O_{21}$ phase (JCPDS card no. 00-050-0445) [43] and unreacted Pb (JCPDS card no. 00-0004-0686) [44].

The microstructural SEM images of PFN–F material obtained by conventional method and SPS technology are presented in Fig. 2. In the first and second technologies, the fracture microstructure of the sample shows a high degree of sintering. The ceramic grains are strongly grown together to form a monolithic structure. In Fig. 3, the SEM images made in the BSE technique (backscattered) are presented, which are equivalent to the microstructural images presented in Fig. 2. The BSE mode detects the secondary electrons mixed with a variable fraction of the BSE backscattered electrons what is well visible for PFN–F composites. The test results showed that the grains of the magnetic component (ferrite) are surrounded by grains of the ferroelectric component (PFN). In the case of SPS (SPSc sample) sample, the ferrite grains grow more slowly (significantly smaller grains of the ferrite component—dark grains) than in the case of a sample obtained in conventional technology (CMc sample). In the SPSc sample, the ferrite grains are clearly smaller—but there are both fine and large ferrite grains in the microstructure, and they are distributed in the structure in an uneven manner (Fig. 4). As for the matrix of composite samples (ferroelectric PFN material—light ceramic grains), the grain size is similar for both technologies.

The temperature tests for the dielectric permittivity showed that the composite CMc sample has high values of ε both at room temperature and at the phase transition temperature (Fig. 5a).

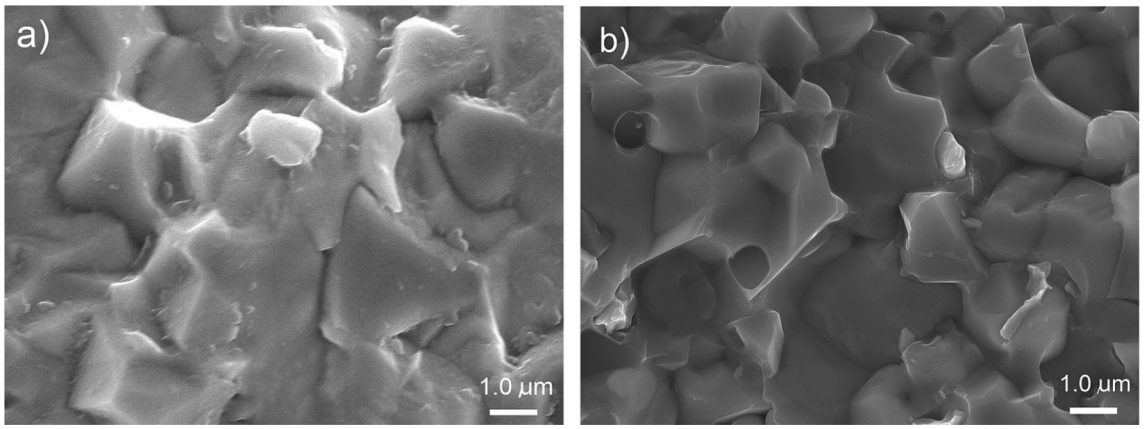

Fig. 2 SEM images of the microstructure of fracture of the PFN–F samples: CMc sample (**a**) and SPSc sample (**b**), at the standard SB mode

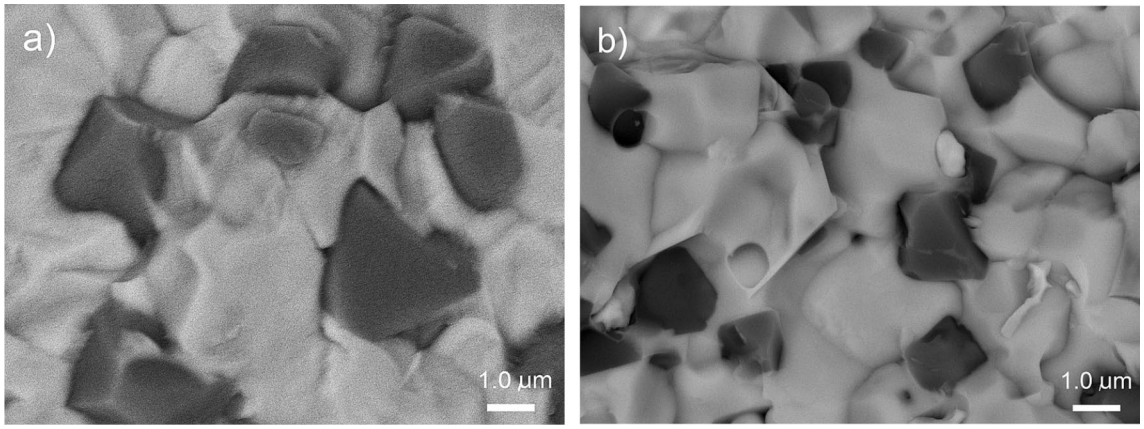

Fig. 3 BSE images of the microstructure of fracture of the PFN–F samples: CMc sample (**a**) and SPSc sample (**b**)

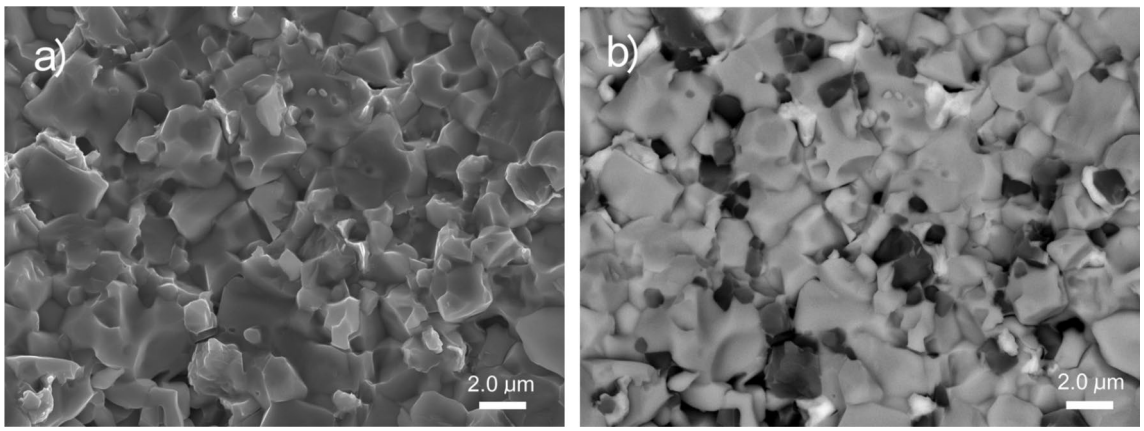

Fig. 4 SEM images of the microstructure of fracture of the SPSc sample: **a** at the standard SB mode, (**b**) at the BSE technique (×5000).

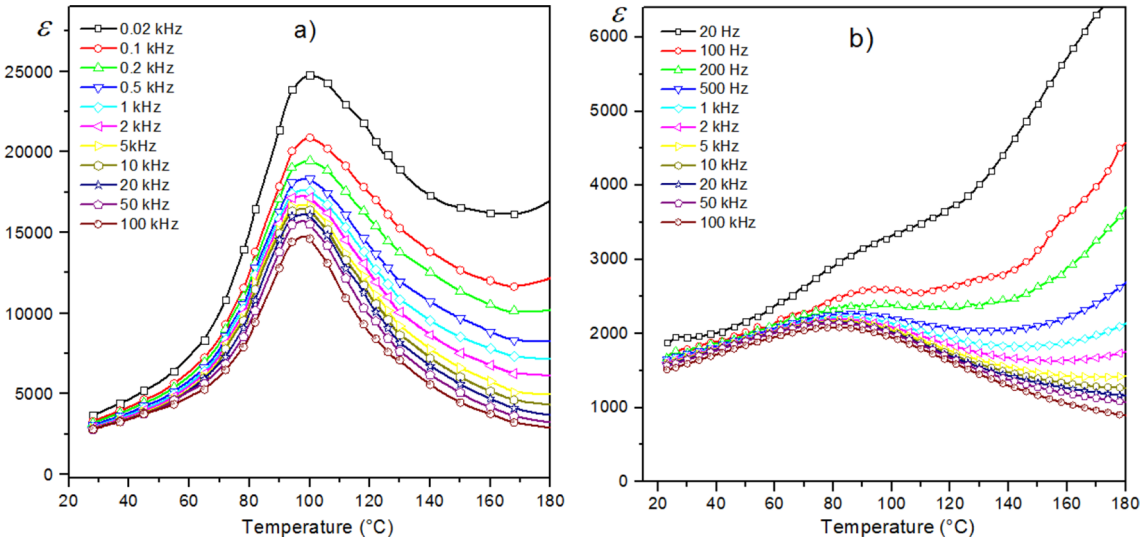

Fig. 5 The $\varepsilon(T)$ temperature relationships for multicomponent PFN–F composites: CMc sample (**a**) and SPSc sample (**b**)

The phase transition (from the ferroelectric phase to the paraelectic phase) takes place in a narrow temperature range. With the measuring field frequency increase (20 Hz to 100 kHz), the phase transition temperature (T_C where there is ε_{max}) slightly shifts towards lower temperatures.

In the case of SPS technology, a significant reduction in the dielectric permittivity value (Fig. 5b) of the PFN–F composite sample is observed. The phase transition occurs at a lower temperature and in a much wider temperature range.

The diffuse phase transition occurring in ceramic materials with perovskite structure depends on various factors, for example, chemical composition fluctuations or cation crystallographic site disordering, leading to a microscopic heterogeneity in the composition (are formed microareas as the centers of new phase with different local Curie points) as well as the heterogeneous defect distribution and mechanical stress in the ceramic grains [45]. Lowering the value of electric permittivity and increasing diffuse phase transition of the PFN–F composite obtained in the SPS method may be associated with too fast dynamics of the ongoing process, which causes the heterogeneity of defect distribution and mechanical stress in the ceramic grains. Such a phenomenon also requires the optimization of technological conditions during SPS process.

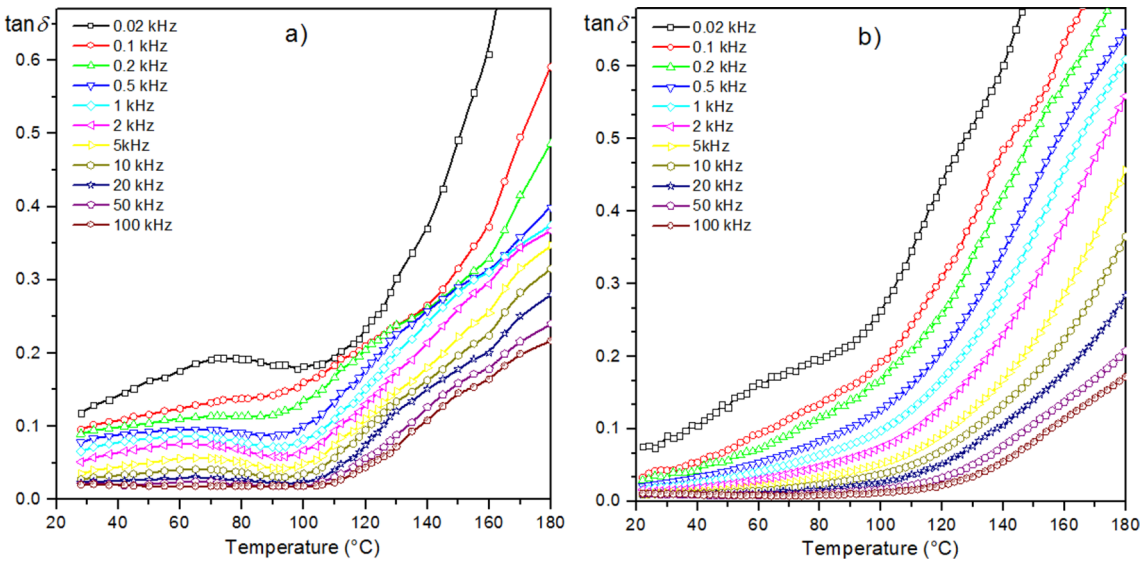

Fig. 6 Temperature dependences of the tanδ for the multicomponent PFN–F composites: CMc sample (**a**) and SPSc sample (**b**)

The temperature dependence of tan$\delta(T)$ for composite PFN–F samples is shown in Fig. 6.

At room temperature, the ceramic sample obtained by SPS has lower dielectric loss.

As the temperature rises, the dielectric losses increase continuously. In the both samples obtained with two different technologies, low dielectric loss is observed up to about 100 °C. Above the phase transition, the increase in dielectric loss takes place in a rapid manner, which is associated with an increase in electrical conductivity at high temperatures.

The test for temperature dependence of electrical conductivity (Fig. 7) shows that the samples have similar curve shapes ln$\sigma_{DC}(1000/T)$. The slightly lower electrical conductivity, throughout the entire measurement area, is obtained in the sample synthesized in SPS technology. The activation energies E_a were calculated for the low- and high-temperature regions, and the values are given in Table 1.

The ferroelectric hysteresis loops of ceramic composite samples obtained at RT and at maximum external electric field ± 3.0 kV/mm are shown in Fig. 8. In the case of the CMc composite obtained with classical technology, the hysteresis loop is pulled out, with a non-standard shape. The coercive field E_C is 0.92 kV/mm, while the remnant polarization P_r is 20.67 μC/cm^2. In the case of the CMc sample, the hysteresis loop shows a similar shape to the results presented in [23] with a similar residual polarization value and a slightly higher coercive field value.

The composite sample obtained in SPS technology has a ferroelectric hysteresis loop without saturation that is a characteristic of a material with losses. It shows lower values of the remnant polarization P_r (11.9 μC/cm^2) and the larger coercive field E_C (1.89 kV/mm). The E_c value for the SPSc sample is similar to the value of coercive fields in ceramic samples with a larger amount of ferrite component [23].

Table 1 Values of the parameters of the PFN–F composite samples

	CMc	SPSc
ρ_{DC} at RT (Ωm)	6.72×10^8	3.03×10^8
E_{Act} in I (eV)	0.63	0.58
E_{Act} in II (eV)	0.92	0.93
T_C (°C)[1]	98	86
ε_r at RT[1]	2950	1628
ε_{max} at T_C[1]	17,670	2224
tanδ at RT[1]	0.063	0.016
tanδ at T_C[1]	0.076	0.078
P_r (μC/cm^2) at RT	20.67	6.38/11.9
E_c (kV/mm) at RT	0.92	1.57/1.89
M (emu/g) at RT	5.07	6.21

[1]For $v = 1$ kHz, RT room temperature

The temperature dependence of magnetization M(T), in the external 0.1 T magnetic field, of the CMc and SPSc composite samples is presented in Fig. 9. The temperature magnetic tests of the PFN–F composite confirmed that at room temperature it exhibits magnetic properties, too. In the CMc sample, the higher magnetization values occur, as compared to those in SPSc sample. As the temperature increases, the magnetization decreases monotonically and reaches 5.07 emu/g at room temperature. In the case of the SPSc sample, the magnetization decrease with temperature is not monotonical, but there is a maximum value of M, at $T = -102$ °C). At room temperature, in SPSc sample, the magnetization is equal to M = 6.21 emu/g.

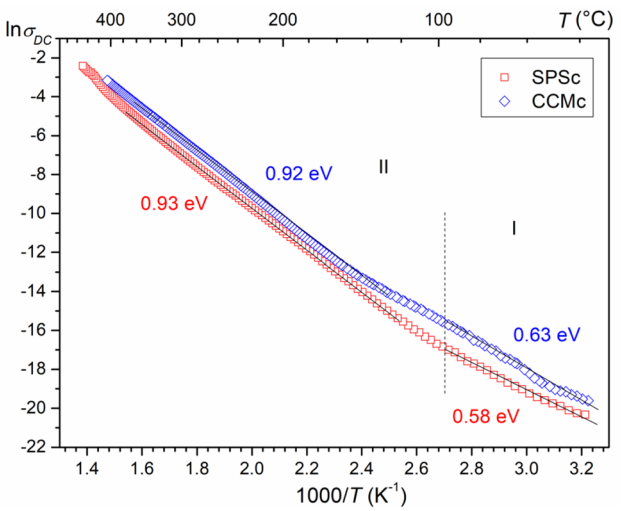

Fig. 7 The ln$\sigma_{DC}(1000/T)$ dependences of the PFN–F composites

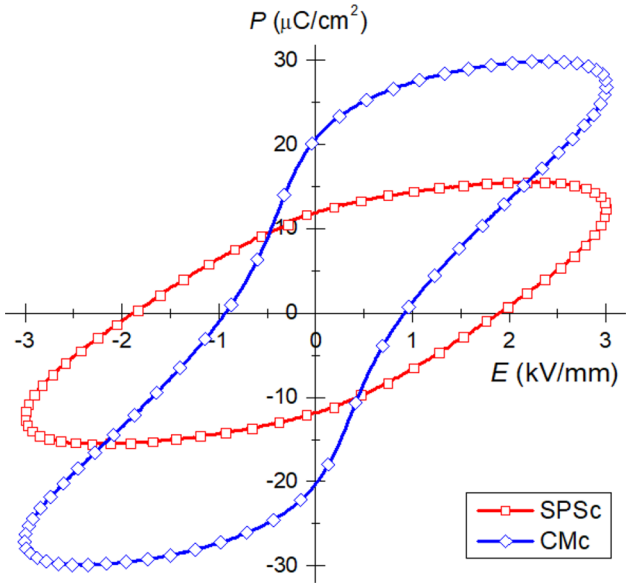

Fig. 8 Hysteresis P–E loops for the PFN–F composites (1 Hz, RT)

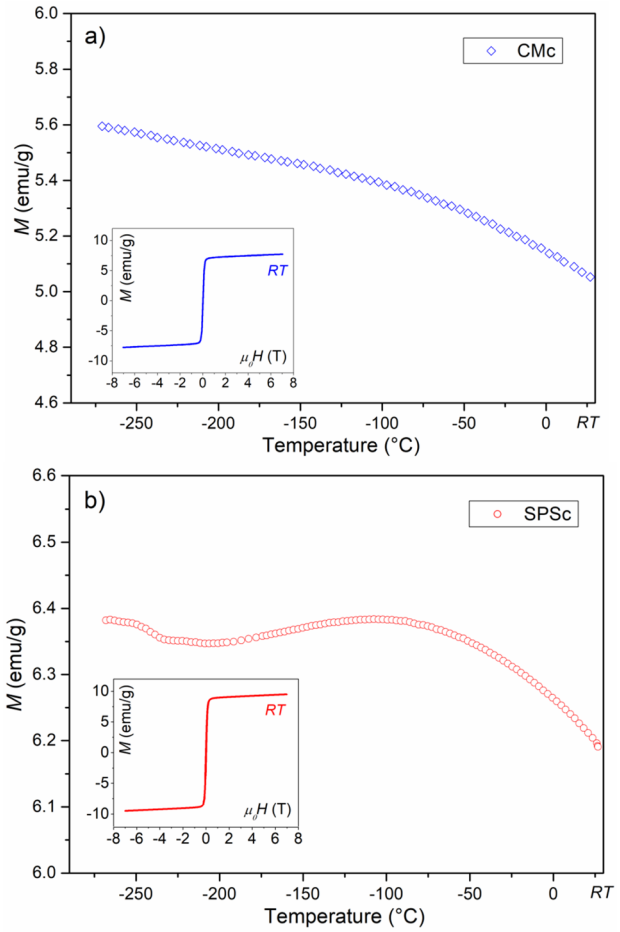

Fig. 9 Dependence of the $M(T)$ for PFN–F composite: **a** CMc, **b** SPSc

The magnetic hysteresis loops made at RT are typical for ferromagnetic soft materials and the saturation is reached at relatively low magnetic fields.

4 Conclusions

In this work, the ceramic composites PFN–F were obtained by the classical sintering and SPS methods. The X-ray analysis showed the occurrence of the strong peaks derived from PFN ferroelectric matrix as well as week peaks coming from the ferrite component without the presence of foreign phases. The tests showed that, at room temperature, the composites exhibit ferroelectric and magnetic properties. The composite sample obtained by the SPS technique not only has lower dielectric loss, but also significantly lower values of the dielectric permittivity, with a highly fuzzy phase transition. According to the latest research, the ceramic materials obtained by SPS are characterized by the most optimal properties than the samples fabricated by other technological methods.

The results of this work, however, showed that the appropriate selection of all process parameters and sintering conditions during SPS technology is crucial to prepare the composite with good properties. Conducting the technology in standard conditions for all materials does not improve the physical properties of the PFN–F composite. This requires further research aimed at the optimization of SPS technology process for composite ceramic samples.

References

1. W. Kleemann, P. Borisov, V.V. Shvartsman, S. Bedanta, EPJ Web Conf. **29**, 00046 (2012)
2. M. Fiebig, T. Lottermoser, D. Meier, M. Trassin, Nat. Rev. Mater. **1**, 16046 (2016)
3. N.A. Spaldin, MRS Bull. **42**, 385 (2017)
4. W. Eerenstein, N.D. Mathur, J.F. Scott, Nature **442**, 759 (2006)
5. N.A. Spaldin, R. Ramesh, Nat Mater. **18**, 203 (2019)
6. J.F. Scott, Nat Mater. **6**, 256 (2007)
7. F. Yang, Y.C. Zhou, M.H. Tang, F. Liu, Y. Ma, X.J. Zheng, W.F. Zhao, H.Y. Xu, Z.H. Sun, J. Phys. D. **42**, 7 (2009)
8. K.F. Wang, J.-M. Liu, Z.F. Ren, Adv. Phys. **58**, 321 (2009)
9. A. Roy, R. Gupta, A. Garg, Adv. Cond. Matter Phys. **2012**, 926290 (2012)
10. D.I. Khomskii, J. Magn. Magn. Mater. **306**, 1 (2006)
11. D.M. Evans, M. Alexe, A. Schilling, A. Kumar, D. Sanchez, N. Ortega, R.S. Katiyar, J.F. Scott, J.M. Gregg, Adv Mater. **27**, 6068 (2015)
12. D.I. Khomskii, Physics **2**, 20 (2009)
13. L. Kozielski, M. Adamczyk, J. Erhart, M. Pawełczyk, J. Electroceram. **29**, 133 (2012)
14. M. Adamczyk, Z. Ujma, L. Szymczak, J. Koperski, Ceram. Int. **31**, 791 (2005)
15. J.F. Scott, J. Mater. Chem. **22**, 4567 (2012)
16. M. Atif, M. Nadeem, R. Grössinger, R.S. Turtelli, J. Alloys Compd. **509**, 5720 (2011)
17. R. Safi, H. Shokrollahi, Prog. Solid State Ch. **40**, 6 (2012)
18. C.-W. Nan, M.I. Bichurin, S. Dong, D. Viehland, G. Srinivasan, J. Appl. Phys. **103**, 031101 (2008)
19. B.-J. Fang, C.-L. Ding, W. Liu, L.-Q. Li, L. Tang, Eur. Phys. J. Appl. Phys. **45**, 20302 (2009)
20. D.K. Pradhan, V.S. Puli, S. Kumari, S. Sahoo, P.T. Das, K. Pradhan, D.K. Pradhan, J.F. Scott, R.S. Katiyar, J. Phys. Chem. C. **120**, 1936 (2016)

21. D.K. Pradhan, S. Sahoo, S.K. Barik, V.S. Puli, P. Misra, R.S. Katiyar, J. Appl. Phys.; **115,** 194105 (2014)
22. D. Bochenek, P. Niemiec, R. Skulski, A. Chrobak, P. Wawrzała, Mater. Chem. Phys. **157**, 116 (2015)
23. D.K. Pradhan, S.K. Barik, S. Sahoo, V.S. Puli, R.S. Katiyar, J. Appl. Phys. **113**, 144104 (2013)
24. K. Osińska, A. Lisińska-Czekaj, H. Bernard, J. Dzik, D. Czekaj, Arch. Metall. Mater. **56**, 1093 (2011)
25. D. Bochenek, P. Niemiec, P. Guzdek, M. Wzorek, Mater. Chem. Phys. **195**, 199 (2017)
26. J.A. Bartkowska, D. Bochenek, J. Mater. Sci.-Mater. El. **29**, 17262 (2018)
27. U. Acevedo-Salas, R. Breitwieser, T. Gaudisson, S. Nowak, S. Ammar, R. Valenzuela, Appl. Phys. A. **123**, 659 (2017)
28. R. Licheri, S. Fadda, R. Orrù, G. Cao, V. Buscaglia, J. Eur. Ceram. Soc. **27**, 2245 (2007)
29. A. Srinivas, M.M. Raja, D. Sivaprahasam, P. Saravanan, Process Appl. Ceram. **7**, 29 (2013)
30. Q. Jiang, F. Liu, H. Yan, H. Ning, Z. Libor, Q. Zhang, M. Cain, M.J. Reece, J. Am. Ceram. Soc. **94**, 2311 (2011)
31. D. Bochenek, P. Niemiec, Materials **11**, 2504 (2018)
32. R. Font, O. Raymond-Herrera, L. Mestres, J. Portelles, J. Fuentes, J.M. Siqueiros, J. Mater. Sci. **51**, 6319 (2016)
33. D. Bochenek, J. Alloys Compd. **504**, 508 (2010)
34. S.I. Raevskaya, S.P. Kubrin, I.P. Raevski, C.C. Chou, H. Chen, V.V. Titov, M.A. Malitskaya, D.A. Sarychev, I.N. Zakharchenko, Ferroelectrics **509**, 64 (2017)
35. D. Bochenek, Z. Surowiak, Phys. Status Solidi A **206**, 2857 (2009)
36. V.V. Laguta, V.A. Stephanovich, I.P. Raevski, S.I. Raevskaya V.V. Titov, V.G. Smotrakov, V.V. Eremkin, Phys. Rev. B. **95,** 014207 (2017)
37. H. Ursic, A. Bencan, U. Prah, M. Dragomir, B. Malic, Materials **12**, 1327 (2019)
38. I.P. Raevski, V.V. Titov, H. Chen, I.N. Zakharchenko, S.I. Raevskaya, S.I. Shevtsova, J. Mater. Sci. (2019). https://doi.org/10.1007/s10853-019-03669-4
39. R. Skulski, P. Wawrzała, K. Ćwikiel, D. Bochenek, J. Intel. Mat. Syst. Str. **18**, 1049 (2007)
40. D. Bochenek, R. Zachariasz, Arch. Metall. Mater. **54**, 903 (2009)
41. F.N.A. Freire, H.H.B. Rocha, M.R.P. Santos, P.B.A. Fechine, F.M.M. Pereira, R.S.T.M. Sohn, I.F. Vasconcelos, A.S.B. Sombra, J. Mater. Sci. **43**, 75 (2008)
42. P. Priyadharsini, A. Pradeep, P. Sambasiva Rao, G. Chandrasekaran, Mater. Chem. Phys. **116**, 207 (2009)
43. M. Ferriol, J.-L. Rivolier, C. Goutaudier, M.-T. Cohen-Adad, Eur. J. Solid State Inorg. Chem. **32**, 263 (1995)
44. T. Swanson. Natl. Bur. Stand. (U.S.), Circ. 539, I, **34** (1953)
45. D. Bochenek, P. Niemiec, G. Dercz, Materials **13**, 1996 (2020)